sustainability

Article

Parameter Robustness Enhanced Deadbeat Control for DFIG with ESO-Based Disturbance Estimation

Kai Ni [1,2], Haochen Shi [2,*], Jin Zhang [1], Chong Zhang [2], Hongzhe Wang [2] and Yizhou Sun [2]

1 State Key Laboratory of Operation and Control of Renewable Energy & Storage Systems, China Electric Power Research Institute, Beijing 100192, China; zhangjin1@epri.sgcc.com.cn (J.Z.)
2 State Key Laboratory of Advanced Electromagnetic Engineering and Technology, The School of Electrical and Electronic Engineering, Huazhong University of Science and Technology, Wuhan 430070, China
* Correspondence: haochenshi@hust.edu.cn

Abstract: Doubly fed induction generators (DFIGs) are widely applied in wind energy conversion systems, where the harsh service environment and long-lasting operation can bring about motor parameter deviations, deteriorating the system performance. In this paper, an extended state observer (ESO)-based deadbeat control strategy that enhances the system parameter robustness is proposed. Firstly, the effects of motor parameter inaccuracy are analyzed to reflect the control errors and degradation of the system performance. Secondly, a lumped disturbance represented by an additional state extended from the system mathematical model is derived with the parameter inaccuracy taken into consideration. Finally, the parameter robustness enhanced deadbeat control method with the ESO-based disturbance estimation is developed to realize accurate prediction and control, even when the inductance of DFIG deviates under various operation conditions. To verify the effectiveness of the proposed method, simulations are carried out in MATLAB/Simulink for a 1.5 MW DFIG with a 30% stator and rotor inductance deviation. Compared to the conventional control method, smooth and fast dynamic performance is maintained, and the current ripple for the proposed control strategy can be reduced by approximately 40%, where the steady-state tracking performance and parameter robustness of the system are significantly enhanced.

Keywords: doubly fed induction generator; wind energy conversion system; parameter deviation; deadbeat control; parameter robustness

check for updates

Citation: Ni, K.; Shi, H.; Zhang, J.; Zhang, C.; Wang, H.; Sun, Y. Parameter Robustness Enhanced Deadbeat Control for DFIG with ESO-Based Disturbance Estimation. *Sustainability* **2023**, *15*, 12020. https://doi.org/10.3390/su151512020

Academic Editor: Nicoletta Matera

Received: 10 June 2023
Revised: 19 July 2023
Accepted: 27 July 2023
Published: 5 August 2023

1. Introduction

With the optimization of energy infrastructure, and the proposal of energy conservation and emission reduction goals, available wind energy has become an indispensable new energy source during the energy evolution due to its wide distribution and environmentally friendly feature [1–3]. A doubly fed induction generator (DFIG) that has the advantages of high efficiency and a low operation cost, as well as the characteristics of variable-speed constant-frequency regulation, active and reactive power decoupling control, and a small converter capacity, is applied widely in the power grid [4–6]. In a DFIG wind turbine, a grid-side converter (GSC) is connected to the grid for keeping the DC-bus voltage stable, and a rotor-side converter (RSC) is connected to the rotor of DFIG to control the electromagnetic torque, and active and reactive power [7].

The traditional control strategies of DFIG mainly consist of vector control (VC), direct torque control (DTC), and direct power control (DPC). For VC, the stator flux or grid voltage orientation is applied for system control, and the decoupling of active and reactive power is realized during this process [8–10]. Direct torque control (DTC) selects the best vector to act on the converter according to the positions of the rotor, electromagnetic torque, and flux linkage vector [11]. Compared with VC, DTC has a faster dynamic response, simpler control structure, and lower dependence on circuit parameters, but the switching frequency is not fixed, and there are large electromagnetic fluctuations [12]. A DTC method based on pulse-width modulation (PWM) is proposed to avoid the above-mentioned problems so that the steady-state performance can be improved [13]. Additionally, a type of predictive DTC scheme is proposed to deal with the parameter dependence issue [14]. Another kind of control method with high dynamic performance is called DPC, which is carried out based on the difference between active/reactive power and the corresponding reference values [15,16]. For the DPC strategy, the optimal output is selected according to the vector switching table through a hysteresis comparison, and the challenges of an unfixed switching frequency and large electromagnetic fluctuations can be eliminated by applying the similar methods proposed in refs. [13,14].

Different from the conventional field-oriented control strategies, model predictive control (MPC) strategies are put forward so that the problems with multiple nonlinear control objectives can be solved by simply defining a cost function [17–20]. In ref. [21], an MPC strategy for DFIG is proposed, where a state equation between the power and rotor voltage is deduced, and the power can be precisely tracked through the proposed method without any error feedback, while the computational burden is high. Apart from the MPC scheme based on a cost function, an additional observer is established for a permanent magnet synchronous motor (PMSM) [22]. The current information is obtained to replace the sampled information of the deadbeat predictive current control (DPCC) on the *dq*-axes, which is effective for dealing with the inconsistency between the *dq* and the inherent zero-sequence parameters.

The system parameter uncertainty issue is unavoidable for motor drive applications, which results in control performance deterioration. A comprehensive review is presented in ref. [23] that focuses on the tolerance analysis, reliability determination, and robustness optimization of motors, drives, and power electronics, modeling uncertainty and optimization based on reliability measures. A fault-tolerant control strategy is proposed in ref. [24] by flexibly changing the winding configuration for the motor drive. In ref. [25], a nonlinear robust jitter-free super-twisted fractional-order terminal sliding mode control (ST-FOTSMC) strategy is proposed. In this case, the super-twisted sliding film control and fractional-order terminal sliding mode control are combined, which eliminates the nonlinearity in the wind energy conversion system. A data-driven predictive control method is proposed in ref. [26], which improves the system performance regarding the stabilization time, voltage/current overshoot, and total stator current harmonic distortion. In addition, a notch filter is applied in the deadbeat control strategy in ref. [27] to extract the *dq* components of the negative-sequence voltage in the three-phase voltages so that the issues caused by an unbalanced load can be avoided. Moreover, various types of extended state observers (ESOs) are developed for sensorless control and disturbance rejection for PMSM applications [28–30], while the investigation of ESO-based control methods for DFIG is rare.

In ref. [31], a sensorless control method with an adaptive framework for DFIG is proposed, which eliminates the dependence on sensors, and prior knowledge of system parameters is no longer required. Moreover, a novel control system is proposed to enhance the dynamic performance of DFIG, and a predictive voltage control (PVC) algorithm is formulated to achieve a fast dynamic response [32]. In ref. [33], a robust predictive stator current control (RPCC) method for DFIG is proposed, and the performance deterioration caused by parameter variations is alleviated by applying the error between the measured and predicted values in both the stator current prediction stage and rotor voltage vector calculation process. Furthermore, a model-free deadbeat predictive control method for DFIG is proposed in ref. [34], which has fast dynamic performance and a fixed switching frequency. The ultralocal model is used to substitute the mathematical model of DFIG, and all the compensation terms are treated as lumped disturbance, which is estimated using an observer. However, a high bandwidth is required for the observer since the disturbances to be estimated have high complexity, which may have negative impacts on the system performance and stability.

In this paper, to enhance the parameter robustness of the MPC for a DFIG wind energy conversion system, a novel ESO-based deadbeat control is put forward. First, the effects of inaccurate motor parameters are analyzed and deduced, which allows us to determine the control errors and the degradation of the system performance. Then, the parameter inaccuracy and other unmodeled parts are treated as the lumped disturbance. An additional state is extended from the mathematical model to represent the lumped disturbance, which is estimated using an ESO. Finally, the calculated reference voltage after disturbance compensation realizes more accurate prediction and control, enhancing the parameter robustness of the DFIG system. Compared to the conventional deadbeat control method for DFIG [35], accurate control of the rotor current and strong robustness can be achieved simultaneously, and stable operation and fast switching between various conditions as the reference signals change are also obtained.

2. Modeling of DFIG

A doubly fed induction generator (DFIG) wind power system is a high-order, multi-variable, nonlinear, strong-coupling, and time-varying system. Therefore, the power decoupling control of DFIG needs to be realized through coordinate transformation, and a mathematical model of DFIG is established to obtain the control target under traditional PI regulation.

2.1. DFIG Steady-State Model

In order to obtain the steady-state equivalent circuit of DFIG, the necessary assumptions are as follows: the stator and the rotor are both in the star configuration, and the rotor parameters are referred to the stator side.

The one-phase steady-state equivalent circuit of DFIG referred to the stator side is illustrated in Figure 1, and the expressions are derived according to the circuit [36].

$$\mathbf{U_s} - \mathbf{E_s} = (R_s + \mathrm{j}\omega_s L_{\sigma s})\mathbf{I_s} \tag{1}$$

$$\frac{\mathbf{Ur}}{s} - \mathbf{E_s} = (\frac{R_r}{s} + \mathrm{j}\omega_s L_{\sigma r})\mathbf{I_r} \tag{2}$$

$$\mathbf{E_s} = \mathrm{j}\omega_s L_m(\mathbf{I_s} + \mathrm{I_r}) \tag{3}$$

where $\mathbf{U_s}$ represents the stator voltage, $\mathbf{E_s}$ represents the induced EMF in the stator windings, R_s represents the stator resistance, $\mathbf{I_s}$ represents the induced stator current, R_r represents the rotor resistance referred to the stator side, $\mathbf{I_r}$ represents the induced rotor current referred to the stator side, ω_s represents the angular frequency of the stator voltages, L_m represents the mutual inductance between the stator and rotor, $L_{\sigma s}$ represents the rotor leakage inductance, and $L_{\sigma r}$ represents the rotor leakage inductance referred to the stator side.

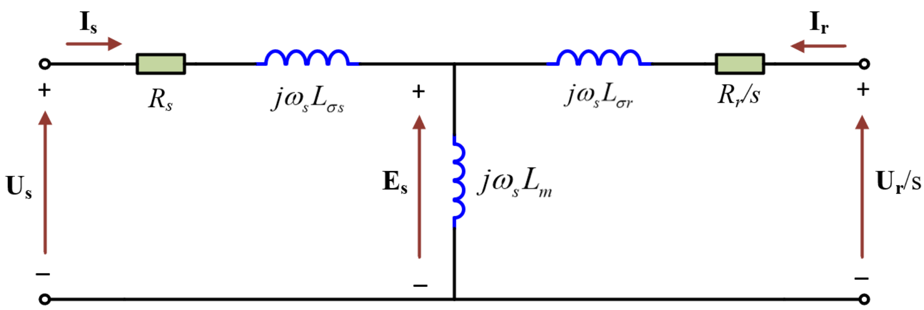

Figure 1. Steady-state equivalent circuit of DFIG referred to the stator side.

The steady-state equivalent circuit of DFIG is obtained according to Thevenin's equivalent theorem. The steady-state voltage equation is also derived, which can be used for a steady-state variable analysis. However, the operation of DFIG in the steady state cannot meet the actual engineering needs. In order to fully understand how DFIG reaches a steady state in different operation modes, a dynamic model is derived, and the dynamic voltage and flux equations are developed.

2.2. DFIG Dynamic Model

Under ideal assumptions, the mathematical model of DFIG in the two-phase synchronously rotating *dq* reference frame can be described according to the following equations [36]:

$$u_{sd} = -R_s i_{sd} - d\psi_{sd}/dt + \omega\psi_{sq} \tag{4}$$

$$u_{sq} = -R_s i_{sq} - d\psi_{sq}/dt - \omega\psi_{sd} \tag{5}$$

$$u_{rd} = -R_r i_{rd} - d\psi_{rd}/dt + (\omega - \omega_r)\psi_{rq} \tag{6}$$

$$u_{rq} = -R_r i_{rq} - d\psi_{rq}/dt - (\omega - \omega_r)\psi_{rd} \tag{7}$$

$$\psi_{sd} = L_s i_{sd} + L_m i_{rd} \tag{8}$$

$$\psi_{sq} = L_s i_{sq} + L_m i_{rq} \tag{9}$$

$$\psi_{rd} = L_m i_{sd} + L_r i_{rd} \tag{10}$$

$$\psi_{rq} = L_m i_{sq} + L_r i_{rq} \tag{11}$$

where u_{sd}, u_{sq}, u_{rd}, and u_{rq} represent the *d*-axis and *q*-axis components of the stator and rotor voltages, respectively; ψ_{sd}, ψ_{sq}, ψ_{rd}, and ψ_{rq} represent the *d*-axis and *q*-axis components of the stator and rotor fluxes, respectively; R_s and R_r represent the stator and rotor resistances, respectively; i_{sd}, i_{sq}, i_{rd}, and i_{rq} represent the *d*-axis and *q*-axis components of the stator and rotor currents, respectively; ω represents the synchronous electrical angular speed; and ω_r represents the rotor electrical angular speed. L_s represents the stator inductance ($L_s = L_{\sigma s} + L_m$), and L_r represents the rotor inductance ($L_r = L_{\sigma r} + L_m$).

Moreover, the torque expression yields

$$T_{em} = \frac{3}{2} p \frac{L_m}{L_s} (\psi_{sq} i_{rd} - \psi_{sd} i_{rq}) \tag{12}$$

3. Conventional Deadbeat Control for DFIG

DFIG is essentially a wound-rotor induction motor, where the basic control principle is consistent with that of other AC machines. The mainstream control methods include vector control, direct torque control, and direct power control, among which vector control is the most widely used. According to the orientation reference, the vector control can be further divided into the rotor-flux-oriented method, the air-gap-flux-oriented method, the stator-flux-oriented method, and the stator-voltage-oriented method.

When adopting the stator-flux-oriented method, the cross-coupling items are relatively few. Correspondingly, the expression of the flux equation is simple, where the direct-axis and quadrature-axis components are the stator flux and zero, respectively. However, the observation accuracy of the stator flux is affected by motor parameters, such as the stator resistance, stator inductance, and mutual inductance. Additionally, the observation is susceptible to magnetic saturation, which limits the reactive power compensation ability of the DFIG system. When using the stator-voltage-oriented method, the above problems are alleviated because the observation of the stator flux is not needed. In this case, the *q*-axis of the synchronous rotating coordinate is oriented in the direction of the stator voltage vector, and the *d*-axis lags the *q*-axis by 90°. Since the stator resistance is very small, by neglecting its effect, Equations (4)–(11) can be modified as [37]

$$0 = -R_s i_{sd} - \frac{d\psi_{sd}}{dt} + \omega\psi_{sq} \tag{13}$$

$$u_s = -R_s i_{sq} - \frac{d\psi_{sq}}{dt} - \omega\psi_{sd} \tag{14}$$

$$u_{rd} = -R_r i_{rd} - \frac{d\psi_{rd}}{dt} + \omega_s\psi_{rq} \tag{15}$$

$$u_{rq} = -R_r i_{rq} - \frac{d\psi_{rq}}{dt} - \omega_s \psi_{rd} \tag{16}$$

where u_s is the amplitude of the stator voltage, and ω_s is the slip angular speed. It can be obtained from Equations (8) and (9) that

$$i_{sd} = \frac{\psi_{sd} - L_m i_{rd}}{L_s}, \quad i_{sq} = \frac{\psi_{sq} - L_m i_{rq}}{L_s} \tag{17}$$

Then, by substituting Equation (17) into Equations (10) and (11),

$$u_{rd} = -(R_r + R_s \frac{L_m^2}{L_s^2}) i_{rd} - \sigma L_r \frac{di_{rd}}{dt} + \sigma \omega_s L_r i_{rq} + \frac{L_m}{L_s} (\frac{R_s}{L_s} \psi_{sd} + \omega_r \psi_{sq}) \tag{18}$$

$$u_{rq} = -(R_r + R_s \frac{L_m^2}{L_s^2}) i_{rq} - \sigma L_r \frac{di_{rq}}{dt} - \sigma \omega_s L_r i_{rq} + \frac{L_m}{L_s} (\frac{R_s}{L_s} \psi_{sq} + \omega_r \psi_{sd}) + \frac{L_m}{L_s} u_s \tag{19}$$

where σ is the leakage coefficiency, which can be calculated as $1 - \frac{L_m^2}{L_s L_r}$. As the stator resistance is relatively small, Equations (18) and (19) can be further simplified as

$$u_{rd} = -R_r i_{rd} - \sigma L_r \frac{di_{rd}}{dt} + \sigma \omega_s L_r i_{rq} + \frac{L_m}{L_s} \omega_r \psi_{sq} \tag{20}$$

$$u_{rq} = -R_r i_{rq} - \sigma L_r \frac{di_{rq}}{dt} - \sigma \omega_s L_r i_{rq} + \frac{L_m}{L_s} \omega_r \psi_{sd} + \frac{L_m}{L_s} u_s \tag{21}$$

It can be seen that the *dq* voltages are composed of the corresponding currents, their derivatives, coupling terms, and other disturbance terms. Hence, the *dq* rotor currents are usually adjusted using the PI controller, and the *dq*-axis decoupling is realized using feedforward compensation. The control diagram is presented in Figure 2.

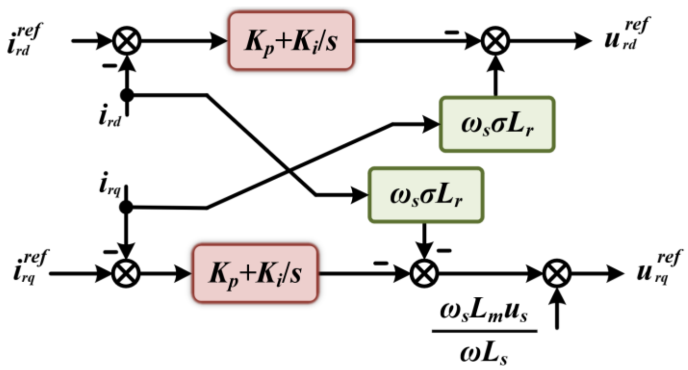

Figure 2. Control diagram of DFIG using PI controller.

However, it takes effort for the parameter tuning of the controller. Additionally, the feedforward compensation for coupling terms plays an important role and cannot be ignored. Thus, the dynamic performance of the DFIG system is limited. To this end, the deadbeat predictive control is introduced to obtain a faster dynamic response [35]. By discretizing Equations (20) and (21), the predictive current in the next period can be given as

$$i_{rd}(k+1) = (1 - \frac{R_r T_s}{\sigma L_r}) i_{rd}(k) - \frac{T_s}{\sigma L_r} u_{rd}(k) + T_s \omega_s i_{rq}(k) + \frac{T_s L_m \omega_r \psi_{sq}}{L_s \sigma L_r} \tag{22}$$

$$i_{rq}(k+1) = (1 - \frac{R_r T_s}{\sigma L_r}) i_{rq}(k) - \frac{T_s}{\sigma L_r} u_{rq}(k) - \omega_s T_s i_{rd}(k) + \frac{L_m T_s \omega_r \psi_{sd}}{\sigma L_r L_s} + \frac{L_m T_s u_s}{\sigma L_r L_s} \tag{23}$$

where "k" and "$k + 1$" denote the variables in the present and the next periods, respectively. Based on the deadbeat principle, supposing that the *dq* currents track the reference ones in the next period, i.e., $i_{rd}(k+1) = i_{rd}^{ref}(k)$ and $i_{rq}(k+1) = i_{rq}^{ref}(k)$, the corresponding dq voltages that need to be applied in the $(k + 1)$th period are

$$u_{rd}^{ref}(k+1) = -R_r i_{rd}(k) - \sigma L_r \frac{i_{rd}^{ref}(k) - i_{rd}(k)}{T_s} + \sigma\omega_s L_r i_{rq}(k) + \frac{L_m}{L_s}\omega_r\psi_{sq} \quad (24)$$

$$u_{rq}^{ref}(k+1) = -R_r i_{rq}(k) - \sigma L_r \frac{i_{rq}^{ref}(k) - i_{rq}(k)}{T_s} - \sigma\omega_s L_r i_{rd}(k) + \frac{L_m}{L_s}\omega_r\psi_{sd} + \frac{L_m}{L_s}u_s \quad (25)$$

where $u_{rd}^{ref}(k+1)$ and $u_{rq}^{ref}(k+1)$ denote the dq-axis reference voltages, respectively. In steady-state operation, the amplitude and frequency of the grid voltage can be considered constant. Thus, $\psi_{sd} = -\frac{u_s}{\omega}$, and $\psi_{sq} = 0$, and Equations (24) and (25) can be converted to

$$u_{rd}^{ref}(k+1) = -R_r i_{rd}(k) - \sigma L_r \frac{i_{rd}^{ref}(k) - i_{rd}(k)}{T_s} + \sigma\omega_s L_r i_{rq}(k) \quad (26)$$

$$u_{rq}^{ref}(k+1) = -R_r i_{rq}(k) - \sigma L_r \frac{i_{rq}^{ref}(k) - i_{rq}(k)}{T_s} - \sigma\omega_s L_r i_{rd}(k) + \omega_s \frac{L_m u_s}{L_s \omega} \quad (27)$$

It can be derived from Equations (26) and (27) that, with accurate parameters, the rotor currents will track the reference ones in the next period once the reference voltage is applied.

Nevertheless, from the calculation of reference voltages, the deadbeat control can be regarded as the proportional control with feedforward compensation. When the parameters are less accurate, the obtained reference voltages will deviate from the ideal values. This may result in distorted phase currents and deteriorated torque performance. Moreover, because there is no integration term, the tracking error exists, leading to the quality decline of the power generation. To solve this problem, a parameter-robust deadbeat control for the DFIG system is proposed.

4. Proposed ESO-Based Deadbeat Control for DFIG

As illustrated above, the model predictive control has been extended to the DFIG system due to its advantages of high dynamic performance, easy implementation, and simple control principle. In addition, benefitting from the modulation process, the current ripple is lower, and the output torque performance is better when adopting the deadbeat control. However, in this case, the system performance is highly dependent on the accuracy of the model. When the model parameters are less accurate, or the actual parameters of the motor change with the operation, serious current distortions and even system oscillation may occur.

Moreover, in the traditional deadbeat control, the predictive model is established based on an approximate simplification of the DFIG system. Hence, many items such as unmodeled parts and disturbances are still not included when establishing the predictive model. To be more specific, the dead-time effect and the voltage drop of power switches, the cross-coupling of dq-axis components, the controller and driver delay, the cogging torque, and other factors are often ignored when establishing the traditional predictive model. This makes the prediction less reliable and ultimately degrades the system's performance. Considering the parameter inaccuracy and the unmodeled parts, the detailed analysis is as follows.

Among all the parameters in the drive system, it is reported in ref. [38] that the motor inductance is most likely to deviate in the DFIG system, including the stator and rotor inductance. To simplify the analysis, the deviation of rotor inductance is discussed as an example. Denoting that L'_{rd} and L'_{rq} are the utilized parameters in the predictive model, and h_{rd} and h_{rq} are the lumped effects from unmodeled parts. Then, the reference voltages obtained using the deadbeat principle are

$$u'_{rd}(k+1) = -R_r i_{rd}(k) - \sigma' L'_r \frac{i_{rd}^{ref}(k) - i_{rd}(k)}{T_s} + \sigma' \omega_s L'_r i_{rq}(k) + h_{rd}(k) \tag{28}$$

$$u'_{rq}(k+1) = -R_r i_{rq}(k) - \sigma' L'_r \frac{i_{rq}^{ref}(k) - i_{rq}(k)}{T_s} - \sigma' \omega_s L'_r i_{rd}(k) + \frac{\omega_s L_m}{\omega L_s} u_s + h_{rq}(k) \tag{29}$$

where σ' is the corresponding leakage coefficient, which is $1 - \frac{L_m^2}{L_s L'_r}$. Compared with the reference voltage obtained under the accurate model, the obtained reference voltage with less accurate parameters can be expressed as

$$u'_{rd}(k+1) = u_{rd}^{ref}(k+1) \underbrace{- \Delta e \cdot \frac{i_d^{ref}(k) - i_{rd}(k)}{T_s} + \Delta e \cdot \omega_s i_{rq}(k) + h_{rd}(k)}_{\Delta u_{rd}(k)} \tag{30}$$

$$u'_{rq}(k+1) = u_{rq}^{ref}(k) \underbrace{- \Delta e \cdot \frac{i_{rq}^{ref}(k) - i_{rq}(k)}{T_s} - \Delta e \cdot \omega_s i_{rd}(k) + h_{rq}(k)}_{\Delta u_{rq}(k)} \tag{31}$$

where $\Delta e = \sigma' L'_r - \sigma L_r$, and Δu_{rd} and Δu_{rq} are the dq reference voltage errors. It can be seen in Equations (28)–(31) that both the parameter inaccuracy and the unmodeled parts lead to the deviation of reference voltages. In consequence, the current harmonics and the torque ripple increase, leading to the deterioration of the system performance. To this end, a novel ESO-based deadbeat control for the DFIG system is put forward, and the concrete principle is presented as follows.

4.1. Disturbance Estimation Principle of ESO

To improve the parameter robustness, the extended state observer is introduced to estimate the system disturbances and unmodeled parts of the system. The disturbance estimation principle is presented below.

By converting the linear system into a state space form, it can be observed that

$$\dot{X} = AX + Bu \tag{32}$$

$$Y = CX \tag{33}$$

where X and Y are the state variable vector and output vector with the dimensions of $m \times 1$ and $n \times 1$, respectively. It should be noted that m and n are the numbers of the system state variables and output variables, respectively. u is the system input; A, B, and C are the system matrix, input matrix, and output matrix with the dimensions of $m \times m$, $m \times m$, and $n \times m$, respectively. Supposing that there exists some uncertainty in the system matrix or input matrix, a new state variable needs to be extended to represent this part. It can be observed that

$$\dot{X} = AX + Bu + z \tag{34}$$

$$\dot{z} = r \tag{35}$$

$$Y = CX \tag{36}$$

where z is an additional extended state variable vector with the dimension of $m \times 1$, and r is the change rate vector of z. Since z is the unknown part, to estimate it, the observer can be established as

$$\dot{\hat{X}} = A\hat{X} + Bu + \hat{z} + L_1(Y - \hat{Y}) \tag{37}$$

$$\dot{\hat{z}} = L_2(Y - \hat{Y}) \tag{38}$$

$$\hat{Y} = C\hat{X} \tag{39}$$

where L_1 and L_2 are the gain parameters. By referring to the equation, both L_1 and L_2 have the dimensions of $m \times n$. It can be seen in Equations (37)–(39) that, when Y approaches its estimated value, the above equation can be simplified as

$$\dot{\hat{X}} = A\hat{X} + Bu + \hat{z} \tag{40}$$

This means that the estimation of z is also approaching the real z. Therefore, the ESO can effectively estimate the extended state of the system in the steady state. At the beginning of the operation, the estimation error is relatively large. However, with the integration process, the estimated values gradually approach the real ones.

In the DFIG system, as shown in Equations (30) and (31), the error resulting from the parameter inaccuracies and unmodeled parts can be considered as the extended state of the system. Then, by using the ESO to estimate the lumped disturbance and compensate it in the predictive model, a more accurate prediction of the system is realized.

4.2. Disturbance Estimation in DFIG Using ESO

As shown in Equations (28)–(31), the parameter inaccuracy and unmodeled parts cause a disturbance in the DFIG system, which eventually leads to the degradation of the system performance. Hence, based on the state space of the dq-axis voltage equation of DFIG, the ESO for the corresponding disturbance estimation is constructed as follows.

Considering the influence of disturbance, the dq-axis voltage equation of DFIG in the continuous domain can be expressed as

$$u_{rd} = -R_r i_{rd} - \sigma L_r \dot{i}_{rd} + \sigma\omega_s L_r i_{rq} + f_{rd} \tag{41}$$

$$u_{rq} = -R_r i_{rq} - \sigma L_r \dot{i}_{rq} - \sigma\omega_s L_r i_{rd} + \frac{\omega_s L_m}{\omega L_s} u_s + f_{rq} \tag{42}$$

where f_{rd} and f_{rq} represent the lumped effect resulting from the disturbances in the dq-axes, respectively. Transforming Equations (41) and (42) to the state space form, the extended state DFIG model can be obtained as

$$\dot{i}_{rd} = -\frac{R_r}{\sigma L_r} i_{rd} + \omega_s i_{rq} - \frac{u_{rd}}{\sigma L_r} + F_{rd} \tag{43}$$

$$\dot{i}_{rq} = -\frac{R_r}{\sigma L_r} i_{rq} - \omega_s i_{rd} - \frac{u_{rq}}{\sigma L_r} + \frac{\omega_s L_m}{\sigma\omega L_r L_s} u_s + F_{rq} \tag{44}$$

where $F_{rd} = -\dfrac{f_{rd}}{\sigma L_r}$, and $F_{rq} = -\dfrac{f_{rq}}{\sigma L_r}$.

After obtaining the extended state dq-axis DFIG model, by referring to Equations (37)–(39), the ESO for the disturbance estimation in the d-axis of DFIG can be designed as

$$e_{rrd} = \hat{i}_{rd} - i_{rd} \tag{45}$$

$$\dot{\hat{i}}_{rd} = -\frac{R_r}{\sigma L_r} \hat{i}_{rd} + \omega_s i_{rq} - \frac{u_{rd}}{\sigma L_r} + \hat{F}_{rd} - \beta_{1d} e_{rrd} \tag{46}$$

$$\dot{\hat{F}}_{rd} = -\beta_{2d} e_{rrd} \tag{47}$$

where $\hat{i}_{rd}$ and $\hat{F}_{rd}$ are the estimated d-axis rotor current and the disturbance, respectively. e_{rrd} is the estimation error of the d-axis rotor current. β_{1d} and β_{2d} are the gain factors of the ESO.

Similarly, the q-axis ESO for the disturbance estimation can be designed as

$$e_{rrq} = \hat{i}_{rq} - i_{rq} \tag{48}$$

$$\dot{\hat{i}}_{rq} = -\frac{R_r}{\sigma L_r} \hat{i}_{rq} - \omega_s i_{rd} - \frac{u_{rq}}{\sigma L_r} + \frac{\omega_s L_m}{\sigma\omega L_r L_s} u_s + \hat{F}_{rq} - \beta_{1q} e_{rrq} \tag{49}$$

$$\dot{\hat{F}}_{rq} = -\beta_{2q} e_{rrq} \tag{50}$$

where $\hat{i}_{rq}$ and $\hat{F}_{rq}$ are the estimation values of the q-axis rotor current and the disturbance, respectively. e_{rrq} is the estimation error of the q-axis rotor current. β_{1q} and β_{2q} are the gain factors of the ESO. It is worth noting that the gain factors are closely related to the bandwidth of the observer. By taking the appropriate values of these gain factors, the estimated currents can quickly track the actual currents. At the same time, the observation of the disturbances is realized.

After the acquisition of the lumped disturbances of the DFIG system, more accurate predictions can be achieved by compensating for the disturbances in the prediction model. This means that the system has a higher robustness to parameters. Correspondingly, the system performance is also improved, as the unmodeled parts are also included.

4.3. Implementation of the Proposed ESO-Based Deadbeat Control on DFIG

To implement the ESO-based deadbeat control in the digital control system, the observer needs to be discretized. Considering the first-order Euler dispersion, the discretized ESO for the d-axis disturbance estimation can be constructed as

$$e_{rrd}(k) = \hat{i}_{rd}(k) - i_{rd}(k) \tag{51}$$

$$\hat{i}_{rd}(k+1) = \hat{i}_{rd}(k) + T_s \begin{pmatrix} -\frac{R_r}{\sigma' L_r'}\hat{i}_{rd}(k) + \omega_s i_{rq}(k) - \frac{1}{\sigma' L_r'} u_{rd}(k) \\ +\hat{F}_{rd}(k) - \beta_{1d} e_{rrd}(k) \end{pmatrix} \tag{52}$$

$$\hat{F}_{rd}(k+1) = \hat{F}_{rd}(k) - T_s \beta_{2d} e_{rrd}(k) \tag{53}$$

where $\hat{i}_{rd}(k)$, $\hat{F}_{rd}(k)$, $e_{rrd}(k)$, $u_{rd}(k)$, and $i_{rd}(k)$ are the estimated d-axis rotor current, the estimated d-axis disturbance, the d-axis current estimation error, the applied d-axis rotor voltage, and the measured d-axis rotor current in the present (k)th period, respectively. $\hat{i}_{rd}(k+1)$ and $\hat{F}_{rd}(k+1)$ are the estimated d-axis rotor current and the estimated d-axis disturbance in the next (k + 1)th period, respectively. It should be noted that, when constructing the ESO in the digital system, accurate parameters are not available. Hence, σ' and $L_r{}'$ rather than σ and L_r are used.

After the observation of the discretized d-axis disturbance, according to Equations (28)–(31) and (51)–(53), the d-axis reference voltage can be calculated as

$$u_{rdc}(k+1) = -R_r i_{rd}(k) + \sigma' L_r' \left(-\frac{i_{rd}^{ref}(k) - i_{rd}(k)}{T_s} + \omega_s i_{rq}(k) - \hat{F}_{rd}(k) \right) \tag{54}$$

where $u_{rdc}(k+1)$ is the compensated d-axis voltage to be applied in the next (k + 1)th period. For the convenience of application, a block diagram of the proposed ESO-based deadbeat rotor current control in d-axis is shown in Figure 3.

Because there are differences between the rotor-side dq-axis voltage equations, the establishment of the corresponding ESOs and compensation for disturbances are introduced separately. The design of the d-axis component of the proposed scheme is derived above, while the corresponding q-axis component is presented below.

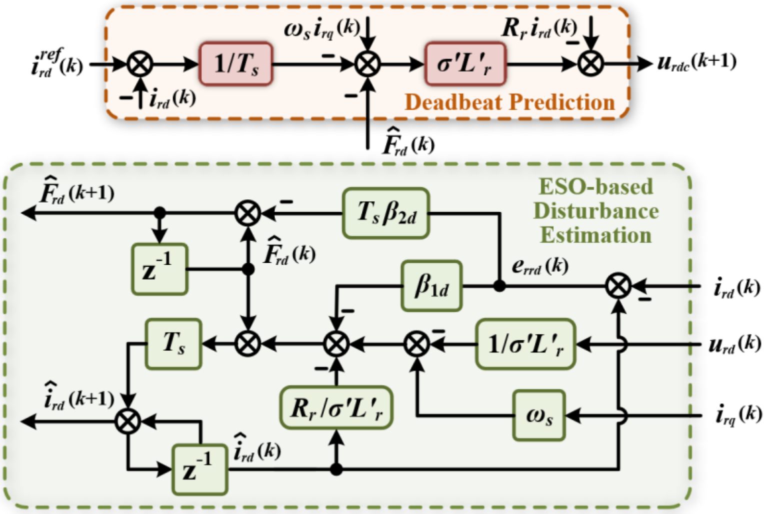

Figure 3. Block diagram of the proposed scheme in *d*-axis.

In this case, by referring to Equations (48)–(50), the ESO for the *q*-axis disturbance estimation is constructed as

$$e_{rrq}(k) = \hat{i}_{rq}(k) - i_{rq}(k) \tag{55}$$

$$\hat{i}_{rq}(k+1) = \hat{i}_{rq}(k) + T_s \left(\begin{array}{c} -\dfrac{R_r}{\sigma' L'_r}\hat{i}_{rq}(k) - \omega_s i_{rd}(k) - \dfrac{1}{\sigma' L'_r}u_{rq}(k) \\ +\dfrac{\omega_s L_m}{\sigma' \omega L'_r L_s}u_s + \hat{F}_{rq}(k) - \beta_{1q}e_{rrq}(k) \end{array} \right) \tag{56}$$

$$\hat{F}_{rq}(k+1) = \hat{F}_{rq}(k) - T_s\beta_{2q}e_{rrq}(k) \tag{57}$$

where $\hat{i}_{rq}(k)$, $\hat{F}_{rq}(k)$, $e_{rrq}(k)$, $u_{rq}(k)$, and $i_{rq}(k)$ are the estimated *q*-axis rotor current, the estimated *q*-axis disturbance, the *q*-axis current estimation error, the applied *q*-axis rotor voltage, and the measured *q*-axis rotor current in the present (*k*)th period, respectively. $\hat{i}_{rq}(k+1)$ and $\hat{F}_{rq}(k+1)$ are the estimated *q*-axis rotor current and the estimated *q*-axis disturbance in the next (*k* + 1)th period, respectively.

After obtaining the discretized *q*-axis disturbance, according to Equations (28)–(57), the *q*-axis reference voltage can be calculated as

$$u_{rqc}(k+1) = -R_r i_{rq}(k) + \sigma' L'_r \left(-\frac{i_{rq}^{ref}(k) - i_{rq}(k)}{T_s} - \omega_s i_{rd}(k) + \frac{\omega_s L_m}{\sigma' \omega L'_r L_s}u_s - \hat{F}_{rq}(k) \right) \tag{58}$$

where $u_{rqc}(k+1)$ is the compensated *q*-axis voltage to be applied in the next (*k* + 1)th period. For the convenience of implementation, a block diagram of the proposed ESO-based deadbeat rotor current control in the *q*-axis is shown in Figure 4.

Moreover, the control instructions are implemented discretely in the digital control system. In other words, when the reference voltages are obtained, they will only take effect in the next period. Hence, the one-step delay is introduced, leading to the deterioration of the control performance. To solve this problem, further estimations and predictions are carried out, where the reference voltages are given by

$$u_{rdc}(k+2) = -R_r i_{rd}(k+1) + \sigma' L'_r \left(-\frac{i_{rd}^{ref}(k+1) - i_{rd}(k+1)}{T_s} + \omega_s i_{rq}(k+1) - \hat{F}_{rd}(k+1) \right) \tag{59}$$

$$u_{rqc}(k+2) = -R_r i_{rq}(k+1) + \sigma' L_r' \left(\begin{array}{l} -\dfrac{i_{rq}^{ref}(k+1) - i_{rq}(k+1)}{T_s} - \omega_s i_{rd}(k+1) \\ +\dfrac{\omega_s L_m}{\sigma' \omega L_r' L_s} u_s - \hat{F}_{rq}(k+1) \end{array} \right) \tag{60}$$

In Equations (32) and (33), the estimation of disturbances and the predicted currents in the $(k+1)$th period, i.e., $\hat{F}_{rd}(k+1)$, $\hat{F}_{rq}(k+1)$, $i_{rd}(k+1)$, and $i_{rq}(k+1)$, are obtained by further performing the estimation and prediction presented in Equations (51)–(58).

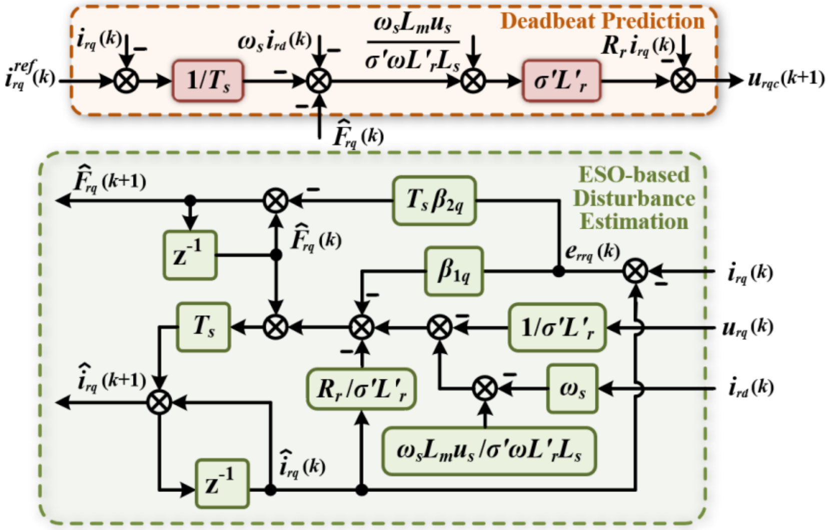

Figure 4. Block diagram of the proposed scheme in q-axis.

5. Simulation Results

In order to validate the effectiveness and robustness of the control strategy proposed in this paper, simulations are conducted in MATLAB/Simulink R2022a for a 1.5 MW DFIG. The nominal parameters of the simulated DFIG system are provided in Table 1. It should be noted that, in the simulations, the active power P_s, reactive power Q_s, electromagnetic torque T_{em}, rotor speed ω, and the DFIG stator and rotor parameters are evaluated in pu, while the DC-bus voltage U_{dc} is evaluated in the respective SI unit (V).

In the simulation, the conventional deadbeat control and the proposed parameter robustness enhanced ESO-based deadbeat control strategy are carried out for a 1.5 MW DFIG, and the step changes in the reference rotor speed and electromagnetic torque are applied to emulate the variations in operating conditions, including wind speed changes. For the control of the grid-side converter, the control signals are derived according to the conventional vector control algorithm. In terms of the rotor-side converter control, the dq voltages to be applied at the $(k + 1)$th instant are calculated according to Equations (26) and (27) in the conventional deadbeat control strategy, which can be regarded as the proportional control with feedforward compensation. Furthermore, when applying the proposed parameter robustness enhanced ESO-based deadbeat control strategy, $i_{rd}(k)$, $i_{rq}(k)$, $u_{rd}(k)$, and $u_{rq}(k)$ are used as the input variables in the ESO-based disturbance estimation module to achieve the estimated d-axis and q-axis disturbances, which are taken into consideration during the calculation process of the compensated dq rotor voltages at both the $(k + 1)$th and $(k + 2)$th instants. Compared with the traditional deadbeat control method, the proposed strategy is capable of compensating the errors caused by the deviations in the stator and rotor inductances.

Table 1. Nominal parameters of the DFIG system.

Parameter	Description	Value
P_n	Rated power	1.5 MW
f_n	Rated frequency	50 Hz
U_{sn}	Stator nominal voltage	575 V
R_s	Stator resistance	0.023 p.u.
L_{ls}	Stator leakage inductance	0.18 p.u.
R_r	Rotor resistance	0.016 p.u.
L_{lr}	Rotor leakage inductance	0.16 p.u.
L_m	Magnetizing inductance	0.29 p.u.
p	Number of pole pairs	3
U_{dcn}	Nominal DC-link voltage	1150 V

In order to comprehensively analyze the steady-state and dynamic performance of the conventional method and the proposed method under various operating conditions, a series of step signals are introduced as the reference ones in the simulation. The basic reference signals are the rotor speed ω_{ref} and electromagnetic torque T_{ref}. The changes in the reference signal levels in the simulation are given in Table 2.

Table 2. Reference signal values set in simulation.

Reference	Value			
time	0–5 s	5–10 s	10–15 s	15–20 s
ω_{ref} (p.u.)	0.9	0.9	1.1	1.1
$\mathrm{T}_{\mathrm{ref}}$ (p.u.)	−0.3	−0.5	−0.5	−0.8

The simulation results of DFIG with matched parameters in the deadbeat control are presented in Figures 5 and 6. Figure 5 shows the waveforms, including the torque, DC-bus voltage, active and reactive power, and rotor and stator currents with the conventional deadbeat control method and the proposed ESO-based deadbeat control method, respectively. It can be seen in the figure that the same steady states under various operating conditions can be achieved with both methods, and stable operation after the switching between different conditions as the reference signals change can be achieved. Moreover, for dynamic performance, as the speed changes, the overshoots of all displayed signals with the proposed control method are significantly reduced compared to those with the conventional method. It can be seen that, when the step change in torque occurs, larger overshoots are encountered compared to the conventional method. However, the overshoots as torque reference signal changes in the proposed control scheme are small enough to be ignored, and a fast dynamic response is maintained.

Figure 5a,b show the performance of the *dq* rotor currents under the defined order of the reference step change (i.e., the signals defined in Table 2) with the conventional deadbeat control method and the proposed ESO-based deadbeat control method, respectively. In order to clearly demonstrate the current tracking performance in the different operating conditions, two typical cases are considered. To be more specific, the situation of 2.5–5.0 s (i.e., ω_{ref} = 0.9 (p.u.), T_{ref} = −0.3 (p.u.)) and the situation of 17.5–20.0 s (i.e., ω_{ref} = 1.1 (p.u.), T_{ref} = −0.8 (p.u.)) are selected to present the operating conditions of "low speed and low power" and "high speed and high power", respectively, which are denoted as cases A and B.

As is presented in Figure 6a, when the conventional deadbeat control scheme is adopted, there are steady-state errors in both the results of the *d*-axis and *q*-axis rotor currents. For case A, the real values of the *dq* rotor currents are always lower than the reference ones, while for case B, the opposite situation occurs. When the proposed ESO-based deadbeat control method is adopted, although the steady-state error of the *q*-axis rotor current is not reduced significantly, the steady-state errors of the *d*-axis rotor current in both cases A and B are eliminated. Moreover, as is indicated in Figure 5, when the speed reference changes, larger current oscillations are introduced compared to the situation when the conventional control method is adopted. However, for the wind energy conversion application, the steady-state performance is much more important than the transient response; thus, the dynamic response is not focused on in this paper, since stable operation after the step change in the reference is guaranteed in the foregoing analysis. Therefore, according to the simulation results in Figures 5 and 6, for the parameter-matched situation, the DFIG system with the proposed control method can effectively work under various operating conditions, and the steady-state tracking accuracy of the *d*-axis current can be greatly improved.

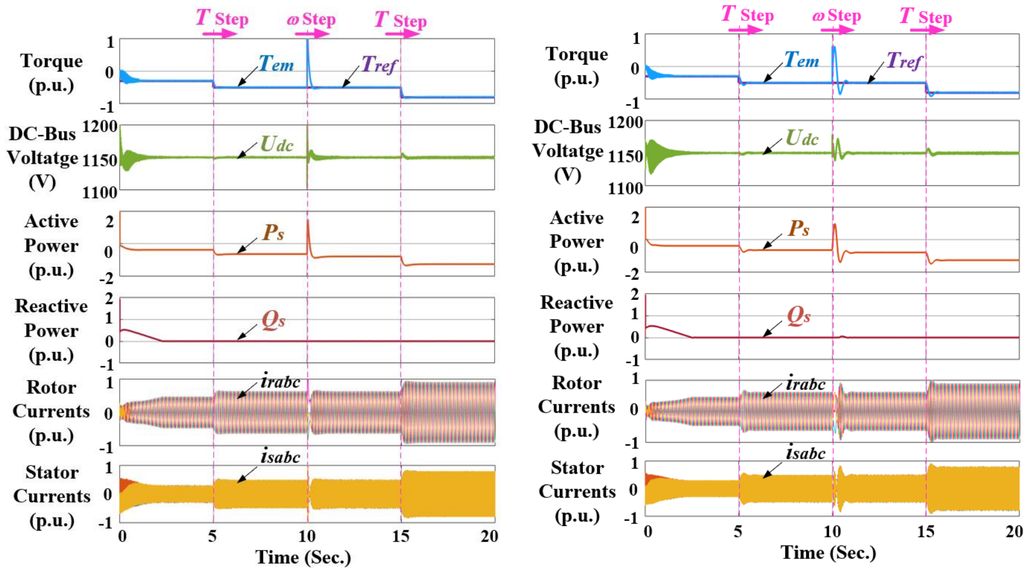

(**a**) (**b**)

Figure 5. Simulation results of a 1.5 MW DFIG system under the defined order of reference step change where the parameters in the deadbeat control are accurate. (**a**) Results of the conventional deadbeat control scheme; (**b**) results of the proposed ESO-based deadbeat control scheme.

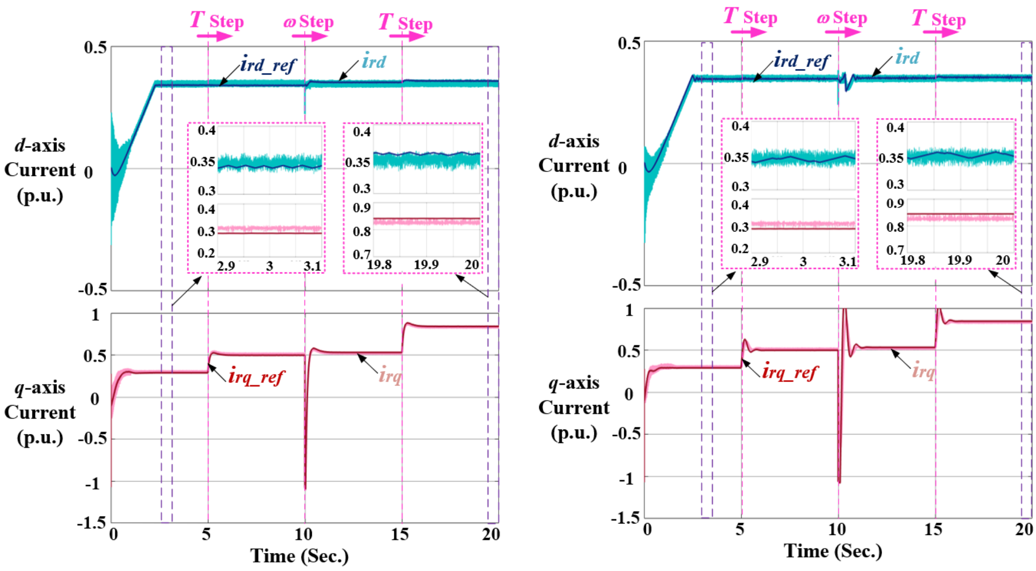

(**a**) (**b**)

Figure 6. *dq* current performance of a 1.5 MW DFIG system under the defined order of reference step change where the parameters in the deadbeat control are accurate. (**a**) Results of the conventional control scheme; (**b**) results of the proposed ESO-based deadbeat control scheme.

The rotor current tracking performance of DFIG with mismatched parameters in the deadbeat control is presented in Figures 7–10. Specifically, two situations of $L_r' = 1.3L_r$ and $L_s' = 1.3L_s$ are taken as examples to represent the parameter-mismatched condition.

The simulation results for cases A and B when $L_r' = 1.3L_r$ are presented in Figures 7 and 8, respectively. According to Figures 7a and 8a, when the conventional deadbeat control method is applied, increased current harmonics and steady-state current errors occur due to parameter mismatch. From Figures 7 and 8, it can be seen that, for both cases A and B, the current harmonics, especially those of the *d*-axis rotor current, are significantly reduced by adopting the proposed ESO-based deadbeat control strategy. Additionally, it can also be observed that the steady-state errors of the rotor current in both cases A and B are greatly reduced. Therefore, with the proposed control method, the rotor current tracking performance can be obviously improved, even when parameter L_r mismatch exists.

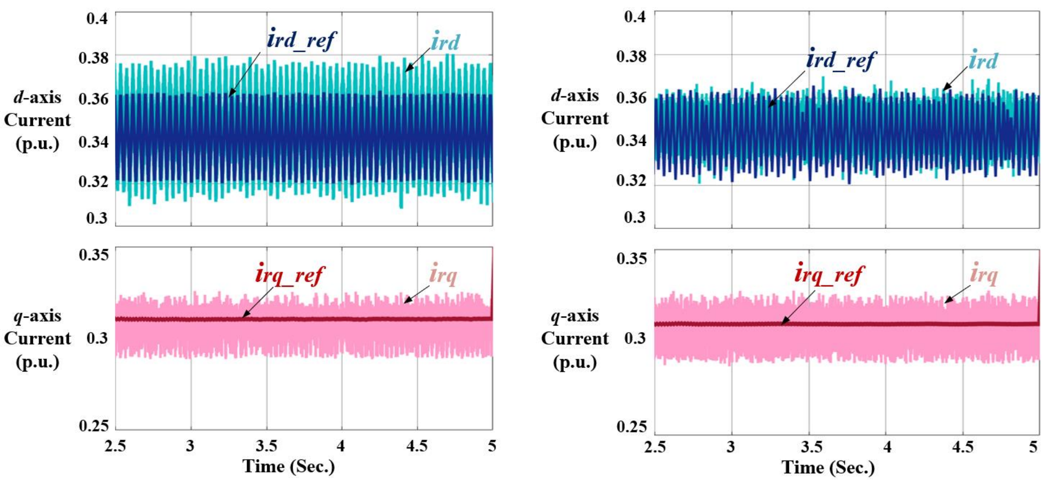

(**a**) (**b**)

Figure 7. *dq* rotor current tracking performance of a 1.5 MW DFIG system in case A when the parameters in the deadbeat control are mismatched ($L_r' = 1.3 \times L_r$). (**a**) Results of the conventional control scheme; (**b**) results of the proposed ESO-based deadbeat control scheme.

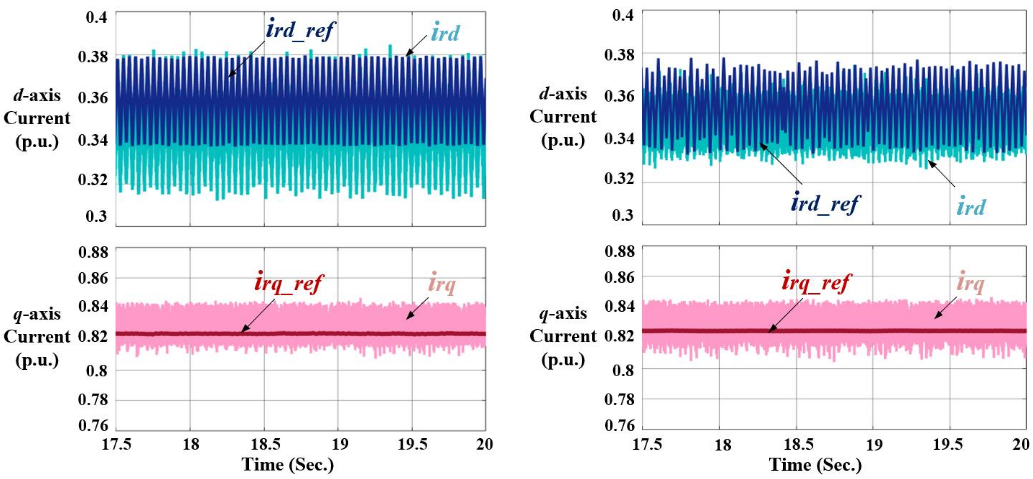

(**a**) (**b**)

Figure 8. *dq* rotor current tracking performance of a 1.5 MW DFIG system in case B, and the parameters in the deadbeat control are mismatched ($L_r' = 1.3 \times L_r$). (**a**) Results of the conventional control scheme; (**b**) results of the proposed ESO-based deadbeat control scheme.

Similarly, when $L_s' = 1.3L_s$, the simulation results for cases A and B with the conventional and the proposed control schemes are presented in Figures 9 and 10, respectively.

According to Figures 9a and 10a, when $L_s' = 1.3L_s$, increased current harmonics and steady-state current errors occur in the conventional control scheme. However, when the proposed control scheme is adopted, the current harmonics, especially those of the *d*-axis rotor current, are significantly reduced in both cases A and B. Additionally, the steady-state errors of the rotor current in both cases A and B are also greatly reduced. Therefore, the rotor current tracking performance can be greatly improved with the proposed control method, and the control system is more robust to parameter mismatch.

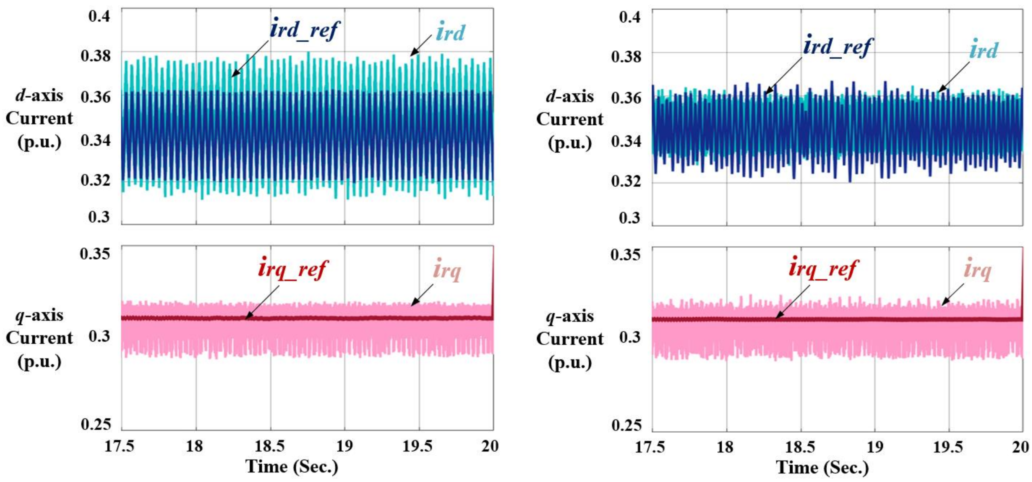

(**a**) (**b**)

Figure 9. *dq* rotor current tracking performance of a 1.5 MW DFIG system in case A, and the parameters in the deadbeat control are mismatched ($L_s' = 1.3 \times L_s$). (**a**) Results of the conventional control scheme; (**b**) results of the proposed ESO-based deadbeat control scheme.

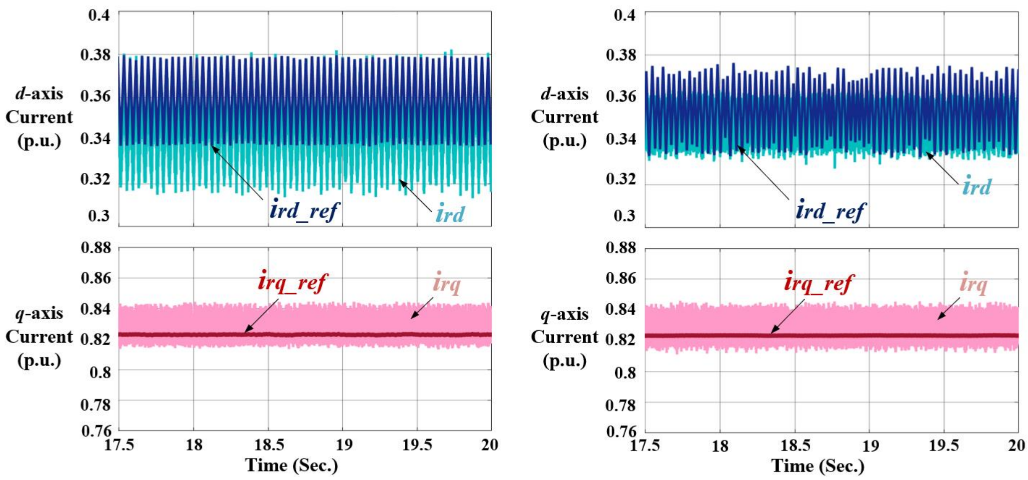

(**a**) (**b**)

Figure 10. *dq* rotor current tracking performance of a 1.5 MW DFIG system in case B, and the parameters in the deadbeat control are mismatched ($L_s' = 1.3 \times L_s$). (**a**) Results of the conventional control scheme; (**b**) results of the proposed ESO-based deadbeat control scheme.

In a word, based on the above analysis, by adopting the proposed control scheme, accurate control of the rotor current and strong robustness can be achieved simultaneously, which validates the effectiveness of the proposed ESO-based deadbeat control strategy. Moreover, stable operation and fast switching between various conditions as the reference signals change are also obtained. Specifically, the overshoots of the currents, dc-bus voltage, and active power can be reduced by 10%, 30%, and 20%, respectively, compared with the traditional deadbeat control method. Furthermore, under the 30% deviation of inductance, the current ripple with the proposed control strategy can be reduced by approximately 40%.

6. Conclusions

In this paper, a parameter robustness enhanced deadbeat control strategy with an ESO-based disturbance estimation is proposed for a DFIG wind energy conversion system. Under the harsh service environment of wind energy conversion systems, motor parameters, such as stator and rotor inductances, are prone to deviate from the originally designed values, which unavoidably deteriorates the system performance. Based on the evaluation of the effects of inaccurate motor parameters on system performance, an ESO is established for the deadbeat control of DFIG to compensate the system disturbance and enhance the parameter robustness. According to the obtained results, the following points are summarized:

1. The transient performance during the speed-change process is significantly improved when applying the proposed method. Specifically, the overshoots of the currents, dc-bus voltage, and active power can be reduced by 10%, 30%, and 20%, respectively.
2. The DFIG system can operate effectively with a high current tracking accuracy under different operating conditions with the proposed strategy.
3. When the proposed control method is applied, the current harmonics are greatly reduced compared to those of the conventional deadbeat control scheme when parameter mismatch is encountered. Specifically, under a 30% deviation of inductance, the current ripple with the proposed control strategy can be reduced by approximately 40%.
4. The proposed parameter robustness enhanced ESO-based deadbeat control strategy of DFIG is highly effective in dealing with the inductance deviation issue, making the wind energy conversion system more adaptive to the harsh service environment.

Author Contributions: Conceptualization, K.N., H.S. and J.Z.; methodology, K.N. and H.S.; software, C.Z., H.W. and Y.S.; validation, K.N., H.S., C.Z. and H.W.; formal analysis, K.N., J.Z. and C.Z.; investigation, H.S. and J.Z.; resources, K.N., J.Z. and Y.S.; data curation, C.Z. and H.W.; writing—original draft preparation, K.N., J.Z. and C.Z.; writing—review and editing, H.S. and H.W.; visualization, K.N.; supervision, K.N. and J.Z.; project administration, H.S. and J.Z.; funding acquisition, J.Z. All authors have read and agreed to the published version of the manuscript.

Funding: This research was supported by Open Fund of State Key Laboratory of Operation and Control of Renewable Energy & Storage Systems (China Electric Power Research Institute), No. NYB51202201703.

Institutional Review Board Statement: Not applicable.

Informed Consent Statement: Not applicable.

Data Availability Statement: Data sharing not applicable.

Conflicts of Interest: The authors declare no conflict of interest.

References

1. Yaramasu, V.; Wu, B.; Sen, P.C.; Kouro, S.; Narimani, M. High-power wind energy conversion systems: State-of-the-art and emerging technologies. *Proc. IEEE* **2015**, *103*, 740–788. [CrossRef]
2. Wu, C.; Zhang, X.-P.; Sterling, M. Wind power generation variations and aggregation. *CSEE J. Power Energy Syst.* **2021**, *8*, 17–38.
3. Hui, J.; Bakhshai, A.; Jain, P. An Energy Management Scheme with Power Limit Capability and an Adaptive Maximum Power Point Tracking for Small Standalone PMSG Wind Energy Systems. *IEEE Trans. Power Electron.* **2015**, *31*, 4861–4875. [CrossRef]
4. Cortes-Vega, D.; Ornelas-Tellez, F.; Anzurez-Marin, J. Nonlinear Optimal Control for PMSG-Based Wind Energy Conversion Systems. *IEEE Lat. Am. Trans.* **2021**, *19*, 1191–1198. [CrossRef]
5. Gururaj, M.V.; Padhy, N.P. PHIL Experimentation on Fault Ride Through Behavior of Doubly Fed Induction Generator-Based Wind System in the Presence of Fault Current Limiter. *IEEE Trans. Ind. Appl.* **2020**, *56*, 2988–3005. [CrossRef]
6. Li, D.; Li, Y.; Zhu, Y.; Pang, G.; Yang, S.; Hu, T. A Novel Control Strategy for the PMSG Wind Turbine Integration with Battery Storage System. In Proceedings of the 2022 12th International Conference on Power and Energy Systems (ICPES), Guangzhou, China, 23–25 December 2022.

7. Li, Y.; Xu, Z.; Zhang, J.; Yang, H.; Wong, K.P. Variable Utilization-Level Scheme for Load-Sharing Control of Wind Farm. *IEEE Trans. Energy Convers.* **2018**, *33*, 856–868. [CrossRef]
8. Prasad, R.M.; Mulla, M.A. Mathematical Modeling and Position-Sensorless Algorithm for Stator-Side Field-Oriented Control of Rotor-Tied DFIG in Rotor Flux Reference Frame. *IEEE Trans. Energy Convers.* **2020**, *35*, 631–639. [CrossRef]
9. Ahmed, M.; Bhattarai, R.; Hossain, S.J.; Abdelrazek, S.; Kamalasadan, S. Coordinated Voltage Control Strategy for Voltage Regulators and Voltage Source Converters Integrated Distribution System. *IEEE Trans. Ind. Appl.* **2019**, *55*, 4235–4246. [CrossRef]
10. Wang, Z.; Wang, Y.; Chen, J.; Hu, Y. Decoupled Vector Space Decomposition Based Space Vector Modulation for Dual Three-Phase Three-Level Motor Drives. *IEEE Trans. Power Electron.* **2018**, *33*, 10683–10697. [CrossRef]
11. Tremblay, E.; Atayde, S.; Chandra, A. Comparative Study of Control Strategies for the Doubly Fed Induction Generator in Wind Energy Conversion Systems: A DSP-Based Implementation Approach. *IEEE Trans. Sustain. Energy* **2011**, *2*, 288–299. [CrossRef]
12. Abad, G.; Rodriguez, M.A.; Poza, J.; Canales, J.M. Direct Torque Control for Doubly Fed Induction Machine-Based Wind Turbines Under Voltage Dips and Without Crowbar Protection. *IEEE Trans. Energy Convers.* **2010**, *25*, 586–588. [CrossRef]
13. Aymen, F.; Mohamed, N.; Chayma, S.; Reddy, C.H.R.; Alharthi, M.M.; Ghoneim, S.S.M. An Improved Direct Torque Control Topology of a Double Stator Machine Using the Fuzzy Logic Controller. *IEEE Access* **2021**, *9*, 126400–126413. [CrossRef]
14. Dan, H.; Zeng, P.; Xiong, W.; Wen, M.; Su, M.; Rivera, M. Model predictive control-based direct torque control for matrix converter-fed induction motor with reduced torque ripple. *CES Trans. Electr. Mach. Syst.* **2021**, *5*, 90–99. [CrossRef]
15. Xu, L.; Cartwright, P. Direct Active and Reactive Power Control of DFIG for Wind Energy Generation. *IEEE Trans. Energy Convers.* **2006**, *21*, 750–758. [CrossRef]
16. Odhano, S.; Rubino, S.; Tang, M.; Zanchetta, P.; Bojoi, R. Stator Current-Sensorless-Modulated Model Predictive Direct Power Control of a DFIM With Magnetizing Characteristic Identification. *IEEE J. Emerg. Sel. Top. Power Electron.* **2021**, *9*, 2797–2806. [CrossRef]
17. Zarei, M.E.; Ramirez, D.; Prodanovic, M.; Venkataramanan, G. Multivector Model Predictive Power Control for Grid Connected Converters in Renewable Power Plants. *IEEE J. Emerg. Sel. Top. Power Electron.* **2022**, *10*, 1466–1478. [CrossRef]
18. Song, W.; Zhong, M.; Deng, Y.; Yin, S.; Yu, B. Model Predictive Power Control for Bidirectional Series Resonant Isolated DC–DC Converters With Steady-State and Dynamic Performance Optimization. *IEEE J. Emerg. Sel. Top. Ind. Electron.* **2022**, *3*, 604–615. [CrossRef]
19. Rodriguez, J.; Garcia, C.; Mora, A.; Flores-Bahamonde, F.; Acuna, P.; Novak, M.; Zhang, Y.; Tarisciotti, L.; Davari, S.A.; Zhang, Z.; et al. Latest Advances of Model Predictive Control in Electrical Drives—Part I: Basic Concepts and Advanced Strategies. *IEEE Trans. Power Electron.* **2022**, *37*, 3927–3942. [CrossRef]
20. Zhang, Y.; Jiang, H.; Yang, H. Model Predictive Control of PMSM Drives Based on General Discrete Space Vector Modulation. *IEEE Trans. Energy Convers.* **2021**, *36*, 1300–1307. [CrossRef]
21. Zhang, Y.; Jiao, J.; Xu, D. Direct Power Control of Doubly Fed Induction Generator Using Extended Power Theory Under Unbalanced Network. *IEEE Trans. Power Electron.* **2019**, *34*, 12024–12037. [CrossRef]
22. Li, X.; Zhang, S.; Zhang, C.; Zhou, Y.; Zhang, C. An Improved Deadbeat Predictive Current Control Scheme for Open-Winding Permanent Magnet Synchronous Motors Drives With Disturbance Observer. *IEEE Trans. Power Electron.* **2021**, *36*, 4622–4632. [CrossRef]
23. Bramerdorfer, G.; Lei, G.; Cavagnino, A.; Zhang, Y.; Sykulski, J.; Lowther, D.A. More Robust and Reliable Optimized Energy Conversion Facilitated through Electric Machines, Power Electronics and Drives, and Their Control: State-of-the-Art and Trends. *IEEE Trans. Energy Convers.* **2020**, *35*, 1997–2012. [CrossRef]
24. Gan, C.; Li, X.; Yu, Z.; Ni, K.; Wang, S.; Qu, R. Modular Seven-Leg Switched Reluctance Motor Drive With Flexible Winding Configuration and Fault-Tolerant Capability. *IEEE Trans. Transport. Electrific.* **2023**, *9*, 2711–2722. [CrossRef]
25. Sami, I.; Ullah, S.; Ali, Z.; Ullah, N.; Ro, J.-S. A Super Twisting Fractional Order Terminal Sliding Mode Control for DFIG-Based Wind Energy Conversion System. *Energies* **2020**, *13*, 2158. [CrossRef]
26. Wei, Y.; Young, H.; Wang, F.; Rodríguez, J. Generalized Data-Driven Model-Free Predictive Control for Electrical Drive Systems. *IEEE Trans. Ind. Electron.* **2023**, *70*, 7642–7652. [CrossRef]
27. Gao, J.; Xu, W.; Liu, Y.; Yu, K. Improved Control Scheme for Unbalanced Standalone BDFIG Using Dead Beat Control Method. In Proceedings of the 2018 IEEE Energy Conversion Congress and Exposition (ECCE), Portland, OR, USA, 23–27 September 2018.
28. Yang, Z.; Miao, C.; Sun, X. Model Predictive Current Control for IPMSM Drives With Extended-State-Observer-Based Sliding Mode Speed Controller. *IEEE Trans. Energy Convers.* **2023**, *38*, 1471–1480. [CrossRef]
29. Wang, Y.; Fang, S.; Huang, D. An Improved Model-Free Active Disturbance Rejection Deadbeat Predictive Current Control Method of PMSM Based on Data-Driven. *IEEE Trans. Power Electron.* **2023**, *38*, 9606–9616. [CrossRef]
30. Zhang, Y.; Yin, Z.; Bai, C.; Wang, G.; Liu, J. A Rotor Position and Speed Estimation Method Using an Improved Linear Extended State Observer for IPMSM Sensorless Drives. *IEEE Trans. Power Electron.* **2021**, *36*, 14062–14073. [CrossRef]
31. Nair, A.R.; Bhattarai, R.; Smith, M.; Kamalasadan, S. Parametrically Robust Identification Based Sensorless Control Approach for Doubly Fed Induction Generator. *IEEE Trans. Ind. Appl.* **2021**, *57*, 1024–1034. [CrossRef]
32. Mossa, M.A.; Abdelhamid, M.K.; Hassan, A.A.; Bianchi, N. Improving the Dynamic Performance of a Variable Speed DFIG for Energy Conversion Purposes Using an Effective Control System. *Processes* **2022**, *10*, 456. [CrossRef]
33. Zhang, Y.; Jiang, T. Robust Predictive Stator Current Control Based on Prediction Error Compensation for a Doubly Fed Induction Generator Under Nonideal Grids. *IEEE Trans. Ind. Electron.* **2022**, *69*, 4398–4408. [CrossRef]

34. Zhang, Y.; Jiang, T.; Jiao, J. Model-Free Predictive Current Control of DFIG Based on an Extended State Observer Under Unbalanced and Distorted Grid. *IEEE Trans. Power Electron.* **2020**, *35*, 8130–8139. [CrossRef]
35. Franco, R.; Capovilla, C.E.; Jacomini, R.V.; Altana, J.A.T.; Filho, A.J.S. A deadbeat direct power control applied to doubly-fed induction aerogenerator under normal and sag voltages conditions. In Proceedings of the IECON 2014—40th Annual Conference of the IEEE Industrial Electronics Society, Dallas, TX, USA, 29 October–1 November 2014.
36. Abad, G.; Lopez, J.S.; Rodriguez, M.A.; Marroyo, L.; Iwanski, G. *Doubly Fed Induction Machine: Modeling and Control for Wind Energy Generation*; Wiley: Hoboken, NJ, USA, 2011.
37. Heng, N.; Yipeng, S. Direct Power Control of Doubly Fed Induction Generator Under Distorted Grid Voltage. *IEEE Trans. Power Electron.* **2014**, *29*, 894–905. [CrossRef]
38. Ahmed, H.M.; Jlassi, I.; Cardoso, A.J.M.; Bentaallah, A. Model-Free Predictive Current Control of Synchronous Reluctance Motors Based on a Recurrent Neural Network. *IEEE Trans. Ind. Electron.* **2022**, *69*, 10984–10992. [CrossRef]